J|A|C|S
ARTICLES
Published on Web 05/03/2002

Electroluminescent Zinc(II) Bis(8-hydroxyquinoline): Structural Effects on Electronic States and Device Performance

Linda S. Sapochak,*,† Flocerfida E. Benincasa,† Richard S. Schofield,† Joseph L. Baker,‡ Krystal K. C. Riccio,† Daniel Fogarty,† Holger Kohlmann,‡ Kim F. Ferris,§ and Paul E. Burrows§

Contribution from the Departments of Chemistry and Physics, University of Nevada Las Vegas, Las Vegas, Nevada 89154, and Pacific Northwest National Laboratory, Richland, Washington 99352

Received February 5, 2002

Abstract: We present direct evidence for stable oligomers in vacuum-deposited thin films of zinc(II) bis-(8-hydroxyquinoline) (Znq_2). The tetramer [$(Znq_2)_4$] is the energetically favored configuration in both the single crystal and the vacuum-deposited thin film. Oligomerization leads to distinct, symmetry-driven differences between the electronic states in Znq_2 and those in the archetypal organic electroluminescent molecule tris(8-hydroxyquinoline) aluminum (Alq_3). In the case of the Znq_2 tetramer, symmetry leads to an extended network of overlapping pyridyl and phenolato moieties in the solid film. Analysis of the electronic structure of $(Znq_2)_4$ calculated by ab initio Hartree−Fock (HF) methods reveals a localization and energy shift of high-lying occupied and low-lying unoccupied states on symmetry related ligands located on opposite sides of the supramolecular structure resulting in a dipole moment for $(Znq_2)_4$ tetramer close to zero. The optimal π-overlap pathways, altered charge distributions, and extended electronic states of tetrameric Znq_2 may be expected to enable low operating voltage organic light-emitting devices (OLEDs) based on Znq_2. We present preliminary evidence that the operating voltage of $(Znq_2)_4$-based OLEDs is indeed lower than that of identical devices made with Alq_3. Strategic substitution of 8-hydroxyquinoline ligands and control of the structural symmetry of the corresponding metal chelates may offer a route to high efficiency and low operating voltage small molecule OLEDs.

Introduction

Metal 8-hydroxyquinoline (Mq_n) chelates have been extensively studied in analytical chemistry.[1] More recently, Alq_3 has been widely used as the emissive and electron transporting material in organic light-emitting devices (OLEDs).[2,3] Despite its ubiquity, this molecule is at best a "good compromise" for OLED applications. The spherical shape of the molecule, which results from the distorted octahedral geometry of the 8-hydroxyquinoline ligands surrounding the Al^{3+} ion center, results in low photoluminescence (PL) quenching in the solid state, measurable (though small) electron mobility, and good stability against recrystallization of the amorphous thin film.

Originally it was believed that the good stability of Alq_3 in vapor-deposited films could be attributed to the presence of a mixture of two geometric isomers, meridianal (*mer*) and facial (*fac*), which have different symmetries (C_1 and C_3 points groups, respectively).[3] Both isomers are chiral, further complicating the possible mixture with optical isomers as well. Schmidbaur proposed, based on variable-temperature solution ^{1}H NMR studies, that both isomers may exist through a ligand equilibrating process resulting from Al−N bond breaking and reforming at elevated temperatures.[4] Theoretical calculations comparing the *mer* and higher symmetry *fac* isomers of Alq_3 showed that the latter was higher in energy by ∼4 kcal/mol, where the authors suggested that if *fac*-Alq_3 was present in vapor-deposited films utilized in OLEDs, it may act as an electron trap.[5] However, infrared spectroscopy[6] and X-ray diffraction studies[7] of Alq_3 showed no evidence for the presence of the *fac* isomer. However, a recent report of a new polymorphic phase of Alq_3 proposed that the *fac* isomer was present in a small amount.[8] Therefore, there is some disagreement in regards to the "isomeric" purity of Alq_3 thin films, but all discussions, including work presented here, refer to *mer*-Alq_3 when describing correlations of structure to electroluminescence performance.

* Corresponding author. E-mail: sapochal@unlv.edu.
† Department of Chemistry, University of Nevada Las Vegas.
‡ Department of Physics, University of Nevada Las Vegas.
§ Pacific Northwest National Laboratory.

(1) Hollingshead, R. G. W. *Oxine and its Derivatives*; Butterworths: London, 1954; Vols. I−IV.
(2) Tang, C. W.; VanSlyke, S. A. *Appl. Phys. Lett.* **1987**, *51*, 913.
(3) Chen, C. H.; Shi, J. *Coord. Chem. Rev.* **1998**, *171*, 161.
(4) Schmidbaur, H.; Lattenbauer, J.; Dallas, L.; Muller, W. G.; Kumberger, O. *Z. Naturforsh.* **1991**, *46b*, 901.
(5) Curioni, A.; Boero, M.; Andreoni, W. *Chem. Phys. Lett.* **1998**, *294*, 263.
(6) Kushto, G. P.; Iizumi, Y.; Kido, J.; Kafafi, Z. H. *J. Phys. Chem.* **2000**, *104*, 3670.
(7) Brinkmann, M.; Gadret, G.; Muccini, M.; Taliani, C.; Masciocchi, N.; Sironi, A. *J. Am. Chem. Soc.* **2000**, *122*, 5147.
(8) Braun, M.; Gmeiner, J.; Tzolov, M.; Coelle, M.; Meyer, F. D.; Milius, W.; Hellebrecht, H.; Wendland, O.; von Schutz, J. U.; Brutting, W. *J. Chem. Phys.* **2001**, *114*, 9625−9632.

For Alq_3 and other Mq_3 (M = Al^{3+}, Ga^{3+}, In^{3+}) chelates, weak molecular interactions result in only small changes in photophysical properties between isolated or solvated molecules and vacuum-deposited amorphous thin films.[9−11] Indeed, semiempirical modeling has been used to demonstrate that, in the Alq_3 system, the molecular orbitals which govern electroluminescence (EL) are localized on individual quinolate ligands.[10] Later investigations of the electronic structure of *mer*-Alq_3 with density functional theory (DFT)-based calculations, X-ray photoemission (XES), and near-edge X-ray absorption fine structure (NEXAFS) support this conclusion with only minor discrepancies.[5,12] Despite the resulting opportunity to use molecular level chemical modification to optimize organic EL, detailed studies of other Mq_n chelates for OLED applications have been relatively sparse[3,9,11,13−15] and attempts to improve on the properties of Alq_3 have met with limited success. In particular, early optimism that 4-methyl substitution of Alq_3 increased the EL quantum efficiency[16] was later tempered by studies which revealed a concomitant, and offsetting, increase in the device operating voltage.[14] This was explained in terms of decreased overlap between unoccupied electronic sites on adjacent pyridyl moieties, leading to decreased efficiency of electron transport. The electronic structure of other Mq_n chelates, however, is less well studied and likely provides an additional degree of freedom for designing improved molecules for organic EL.

Bis(8-hydroxyquinoline) zinc(II) (Znq_2) has been investigated as an electroluminescent material in vapor deposited films,[17−19] in self-assembled multilayers,[20] and doped into poly(vinylcarbazole).[21] However, no correlation of the structure of Znq_2 to resulting device properties has been established. Previous molecular modeling studies of anhydrous Znq_2 predicted distorted planar or distorted tetrahedral geometries depending on the theoretical method used.[22] The crystal structure of Znq_2 dihydrate has been reported and showed that the 8-hydroxyquinoline ligands were planar.[23] In contrast, Kai et al. showed that anhydrous Znq_2 crystals grown from the vapor phase have a tetrameric structure $(Znq_2)_4$ with two distinct Zn^{2+} ion centers with six- and five-coordinate geometry, respectively.[24] Hopkins et al. also suggested that the Znq_2 may exist as a tetramer when doped into films of poly(vinylcarbazole).[21] This suggests that unlike Alq_3, where there is concern in regards to "isomeric" purity, for Znq_2, one must be concerned about "oligomeric" purity. However, most reports of Znq_2 as an electroluminescent material have not considered the impact of oligomerizaton on the device properties and how they may differ from those of Alq_3.

In this paper, we show that, although the quinolate ligand is common to both Alq_3 and Znq_2, oligomerization of the Zn chelate indeed results in a stable tetrameric configuration [$(Znq_2)_4$]. Furthermore, the symmetry of the tetramer leads to a molecular and electronic structure with significantly different EL properties. The sole existence of the tetrameric phase in Znq_2 purified by temperature gradient sublimation is demonstrated by using powder X-ray diffraction. Theoretical calculations of the total energies of the $(Znq_2)_n$ series (n = 1, 2, 4) show that the tetramer is energetically preferred over both the monomer and the dimer. Differential scanning calorimetry (DSC) supports the sole existence of this phase in both single crystals and amorphous, vacuum-deposited thin films.

An ab initio theoretical treatment of the symmetrical $(Znq_2)_4$ supramolecule shows that the high-lying occupied and low-lying unoccupied orbitals have localized electronic character similar to Alq_3, but because of symmetry these electronic states are located on terminal ligands on opposite sides of the supramolecular structure. Analysis of the solid-state packing reveals that these terminal ligands are involved in strong $\pi-\pi$ stacking, which may be expected to result in enhanced electron transport in OLEDs. The properties of identical OLEDs made with Alq_3 and $(Znq_2)_4$ are compared and a lower drive voltage for $(Znq_2)_4$-based devices is indeed observed. With the exception of Alq_3, this is the first detailed investigation correlating molecular and electronic structure of an 8-hydroxyquinoline metal chelate to electroluminescence performance. The distinct, symmetry-induced differences between the behavior of *mer*-Alq_3 and $(Znq_2)_4$ lend new insight to design rules for improved electroluminescent molecules.

Experimental Section

Materials. Alq_3 (purchased from Aldrich Chemical Co.) and Znq_2 (synthesized and characterized as reported previously[15,25]) were purified by high-vacuum temperature gradient sublimation.[26] Each material was heated incrementally in zone 1 of a three-zone furnace from 100 to 375 °C (Alq_3) and 350 °C $(Znq_2)_4$ at ~10^{-6} Torr over a period of 3 days. Crystalline material was collected from the second zone. The hole transporting material, *N*,*N*′-diphenyl-*N*,*N*′-bis(1-naphthol)-1,1′-biphenyl-4,4′diamine (α-NPD), was purchased in device-grade from Kodak and used without further purification.

Structural Characterization (X-ray Diffraction). X-ray powder diffraction patterns of purified Znq_2 were taken on a Rigaku two-circle diffractometer equipped with a rotating anode X-ray source (ULTRAX Mo Kα radiation) and an image plate detector (Rigaku R-axis 4++). The sample, mixed with silicon powder as an internal standard, was enclosed in a 0.3 mm diameter glass capillary. Diffraction data were collected for 20 h and analyzed with FIT2D.[27] Rietveld refinements were carried out with the program FullProf.98.[28]

(9) Burrows, P. E.; Sapochak, L. S.; McCarty, D. M.; Forrest, S. R.; Thompson, M. E. *Appl. Phys. Lett.* **1994**, *64* (20), 2718.
(10) Burrows, P. E.; Shen, Z.; Bulovic, V.; McCarty, D. M.; Forrest, S. R.; Cronin, J. A.; Thompson, M. E. *J. Appl. Phys.* **1996**, *79* (10), 7991.
(11) Padmaperuma, A. M.S. Thesis, University of Nevada Las Vegas, 2000.
(12) Curioni, A.; Andreoni, W.; Treusch, R.; Himpsel, F. J.; Haskal, E.; Seidler, P.; Heske, C.; Kakar, S.; Van Buuren, T.; Terminello, L. J. *Appl. Phys. Lett.* **1998**, *72* (13), 1575.
(13) Sapochak, L. S.; Burrows, P. E.; Garbuzov, D.; Ho, D. M.; Forrest, S. R.; Thompson, M. E. *J. Phys. Chem.* **1996**, *100*, 17766.
(14) Sapochak, L. S.; Padmaperuma, A.; Washton, N.; Endrino, F.; Schmett, G.; Marshall, J.; Fogarty, D.; Burrows, P. E.; Forrest, S. R. *J. Am. Chem. Soc.* **2001**, *126*, 6500.
(15) Sapochak, L. S.; Benincasa, F. E.; Marshall, J.; Fogarty, D.; Nanayakkara, S. *In Molecules as Components of Electronic Devices*; Lieberman, M. Ed. ACS Symposium Series; American Chemical Society: Washington D.C. in press (2002).
(16) Kido, J.; Iizumi, Y. *Appl. Phys. Lett.* **1998**, *73*, 2721.
(17) Hamada, Y.; Sano, T.; Fujita, N.; Fujii, T.; Nishio, Y.; Shibata, K. *Jpn. J. Appl. Phys.* **1993**, *32*, L514.
(18) Park, S. G.; Jung, E. S.; Cho, S. Y.; Chung, P. J. *Kor. J. Mater. Res.* **1999**, *9*, 564.
(19) Donze, N.; Pechy, P.; Gratzel, M.; Schaer, M.; Zuppiroli, L. *Chem. Phys. Lett.* **1999**, *315*, 405.
(20) Thomsen, D. L., III; Phely-Bobin, T.; Papadimitrakopoulos, F. *J. Am. Chem. Soc.* **1998**, *120*, 6177.
(21) Hopkins, T. A.; Meerholz, K.; Shasheen, S.; Anderson, M. L.; Schmidt A.; Kippelen, B.; Padias, A. B.; Hall, K. H.; Peyghambrian, N.; Armstrong, N. R. *Chem. Mater.* **1996**, *8* (2), 344.
(22) Nicolau, D. V.; Yoshikawa, S. *J. Mol. Graphics Modell.* **1998**, *16*, 83.
(23) Merritt, L. L.; Cady, R. T.; Mundy, B. W. *Acta Crystallogr.* **1954**, *7*, 473.
(24) Kai, Y.; Moraita, M.; Yasuka, N.; Kasai, N. *Bull. Chem. Soc. Jpn.* **1985**, *58*, 1631.
(25) Endrino, F., M.S. Thesis, University of Nevada, Las Vegas, 2001.
(26) Forrest, S. R.; Kaplan, M. L.; Schmidt, P. H. *Annu. Rev. Mater. Sci.* **1987**, *17*, 189.
(27) Hammersley, A. P., FIT2D V9.129 Reference manual v3.1, ESRF report 98HA01T, 1998.

Thermal Analysis. Thermal gravimetric analysis (TGA) and DSC were performed with a Netzsch 449C Simultaneous Thermal Analyzer (STA) system. Temperature and enthalpy calibrations were performed with indium, zinc, tin, and bismuth standards at each heating rate. Pure crystalline samples (5−8 mg) were placed in aluminum pans and heated at various rates (20, 5, 2, and 1 °C/min) under N_2 gas at a flow rate of 50 mL/min.

Computational Methods. The ab initio Hartree−Fock (HF) calculations for *mer*-Alq_3 and Znq_2, its dimer, and its tetramer were performed with the PC version of the GAMESS and Spartan systems of electronic structure programs.[29−31] Molecular geometries were force optimized at the SCF level by using the 3-21G* basis set with C_1 symmetry.[32] Starting geometries for these optimizations were derived from the X-ray crystal structure reported by Kai et al.[24] Orbital amplitude plots were generated with Spartan and Molden[33] at the 0.025 probability level.

Electroluminescence Characterization. Organic light-emitting devices (OLEDs) were fabricated with Alq_3 and $(Znq_2)_4$ as the emissive layer. Devices were grown on glass slides precoated with indium tin oxide (ITO) with a sheet resistance of 15Ω/square. The ITO substrates were cleaned as described previously[14] and exposed to UV-ozone for 10 min before being loaded into a nitrogen glovebox (<1 ppm H_2O, <0.5 ppm O_2) coupled to a multichamber vacuum deposition system. The glovebox-coupled vacuum system permitted manipulation and masking of multiple substrates without exposure to the atmosphere. A 500 Å thick layer of α-NPD was deposited on multiple ITO substrates by thermal evaporation from a baffled Ta crucible at a nominal rate of 1−3 Å/s under a base pressure of $<5 \times 10^{-7}$ Torr which were then removed into the glovebox. Each coated substrate was subsequently reloaded into the vacuum, where a 550 Å thick layer of Mq_n was deposited under similar conditions. A top electrode consisting of a 5 Å thick layer of LiF followed by a 1000 Å thick layer of Al was evaporated (0.5 Å/s and 30−40 Å/s, respectively) through a shadow mask containing 1 mm diameter circular apertures. A quartz crystal oscillator placed near the substrate was used to measure the thickness of the films, which were calibrated ex situ using ellipsometry. Film thickness variation was <2% over the entire substrate, and the measured deviation from device to device was ∼1%. Thus devices made with Alq_3 and Znq_2 were identical in all respects.

Devices were tested in air with an electrical pressure contact made by means of a 25 μm diameter Au wire. Current−voltage characteristics were measured with an Agilent Technologies 4155B semiconductor parameter analyzer, and the EL intensity was measured with a Newport 1830-C optical power meter with a large area photodetector placed directly below the glass substrate. Efficiencies reported are measured directly from the back of the device with no corrections or assumptions regarding the angular dependence of the electroluminescence or the relationship between luminance and quantum efficiency.[16] While this may underestimate the absolute device efficiency due to outcoupling effects, it allows for accurate comparison between devices.

Results and Discussion

I. Molecular Structure and Crystal Packing. The structural parameters for $(Znq_2)_4$ were taken from Kai et al.[24] as starting values for the Rietveld refinement, in which scale factors, background (5th order polynomial), profile (pseudo-Voigt), halfwidth, asymmetry, and lattice parameters were allowed to vary. The X-ray diffraction pattern for Znq_2 purified by high-vacuum gradient temperature sublimation shows good correspondence to the calculated pattern for the tetramer $(Znq_2)_4$ (see Figure 1) suggesting a single crystalline phase for this material.

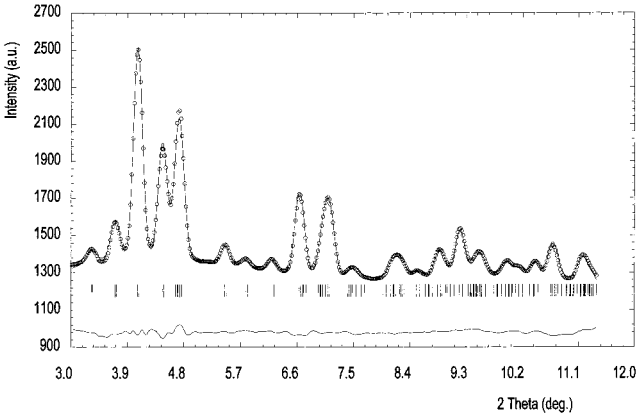

Figure 1. Observed (circles), calculated (solid line), and difference (bottom) X-ray powder diffraction pattern (Mo Kα radiation) with Bragg markers for $[Zn(C_9H_6NO)_2]_4$ or $(Znq_2)_4$. The lattice parameters are refined to $a = 1184.9(3)$ pm, $b = 1302.6(3)$ pm, $c = 1083.8(2)$ pm, $\alpha = 106.55(1)°$, $\beta = 109.06(2)°$, $\gamma = 74.12(2)°$. The residual factors were $R_p = 0.063$ and $R_{wp} = 0.053$; $R_{Bragg} = 0.044$ calculated on the basis of background corrected intensities.

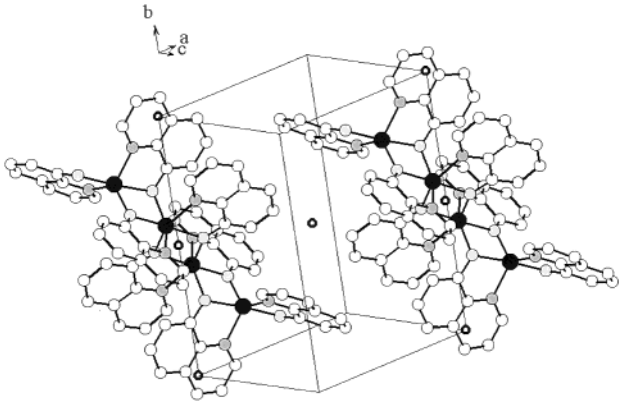

Figure 2. $(Znq_2)_4$ unit cell with Zn atoms (black), O atoms (light gray), N atoms (dark gray), and C atoms (white). Important symmetry inversion centers are indicated with small/empty black circles.

As discussed by Kai et al., $(Znq_2)_4$ contains two crystallographically distinct zinc atoms having different coordination geometries. The zinc atoms [Zn(1)] found on either end of the tetrameric unit are pentacoordinate, resulting in a distorted trigonal bipyramidal geometry, and the central zinc atoms [Zn(2)] are hexacoordinate, resulting in a highly distorted octahedral geometry. Six of the 8-hydroxyquinoline ligands are involved in bridging through the phenolato oxygens, while the remaining two terminal ligands are bound to Zn(1) atoms only.

Unlike *mer*-Alq_3, which lacks symmetry, $(Znq_2)_4$ has a highly symmetrical structure belonging to space group $P\bar{1}$. In the triclinic crystal structure $(Znq_2)_4$ molecules are arranged so that one inversion center is located at the tetramer center and two on either end of the tetrameric unit between terminal, bridging 8-hydroxyquinoline ligands of neighboring $(Znq_2)_4$ molecules (see Figure 2). The former results in an inversion symmetry for the $(Znq_2)_4$ molecule (point group $\bar{1}$), and the latter forces parallel arrangement of the bridging, terminal ligands on adjacent tetrameric units, resulting in a close intermolecular $\pi-\pi$ interaction of 3.37 Å (Figure 3a). These ligands contain the

(28) Rodriguez-Carvajal, J., FullProf98, LLB, 1998.
(29) Schmidt, M. W.; Baldridge, K. K.; Boatz, J. A.; Elbert, S. T.; Gordon, M. S.; Jensen, J. J.; Koseki, S.; Matsunaga, N.; Nguyen, K. A.; Su, S.; Windus, T. L.; Dupuis, M.; Montogomery, J. A. *J. Comput. Chem.* **1993**, *14*, 1347.
(30) PC Spartan Pro, Version 1.0.5, Wavefunction Inc.: Irvine, CA.
(31) Granovsky, A. A. www http://classic.chem.msu.su/gran/gamess/index.html.
(32) Binkley, J. S.; Pople, J. A.; Hehre, W. J. *J. Am. Chem. Soc.* **1980**, *102*, 939. Dobbs, K. D.; Hehre, W. J. *J. Comput. Chem.* **1987**, *8*, 861.
(33) Schaftenaar, G.; Noordik, J. H. *J. Comput.-Aided Mol. Des.* **2000**, *14*, 134 (version 3.7 used).

Table 1. Calculated and Experimental Structural Parameters for $(Znq_2)_4$

structural parameter[a]	exptl[19]	HF/321g*	structural parameter	exptl	HF/3-21g*	structural parameter	exptl	HF/3-21g*
Zn(1)−O(1)	2.072	2.07	O(1)−Zn(1)−O(2′)	105.5	108.9	O(1)−Zn(2)−N(4)	122.4	119.8
Zn(1)−O(2)	2.075	2.04	O(2)−Zn(1)−O(3)	107.6	106.8	O(3)−Zn(2)−N(3)	78.9	79.6
Zn(1)−O(2′)	2.053	1.98	O(2)−Zn(1)−O(2′)	77.0	77.8	O(3)−Zn(2)−N(4)	94.7	100.0
Zn(1)−O(3)	2.163	2.05	O(1)−Zn(1)−N(1)	77.2	76.4	O(4)−Zn(2)−N(3)	97.6	92.8
Zn(1)−N(1)	2.165	2.17	O(1)−Zn(1)−N(2)	101.1	96.0	O(4)−Zn(2)−N(4)	82.4	82.5
Zn(1)−N(2)	2.178	2.19	O(2)−Zn(1)−N(1)	97.7	97.8	N(1)−Zn(1)−N(2)	90.2	84.8
Zn(2)−O(1)	1.965	1.91	O(2)−Zn(1)−N(2)	76.9	76.8	N(1)−Zn(1)−O(2′)	99.4	94.4
Zn(2)−O(3)	2.176	2.11	O(3)−Zn(1)−N(2)	88.8	91.2	N(1)−Zn(1)−O(3)	153.8	153.5
Zn(2)−O(4)	2.020	1.99	O(3)−Zn(1)−O(2′)	93.1	100.2	N(2)−Zn(1)−O(2′)	153.1	154.3
Zn(2)−N(3)	2.047	2.03	O(1)−Zn(2)−O(3)	79.2	80.2	N(3)−Zn(2)−N(4)	116.6	116.8
Zn(2)−N(4)	2.055	2.04	O(1)−Zn(2)−O(4)	106.9	104.9	Zn(1)−O(1)−Zn(2)	106.7	103.7
O(1)−Zn(1)−O(2)	174.5	171.3	O(3)−Zn(2)−O(4)	173.9	172.4	Zn(1)−O(1)−C(17)	116.4	117.3
O(1)−Zn(1)−O(3)	77.3	77.9	O(1)−Zn(2)−N(3)	118.0	122.3	Zn(2)−O(1)−C(17)	136.1	138.7

[a] Bond lengths are reported in angstroms and bond angles in degrees.

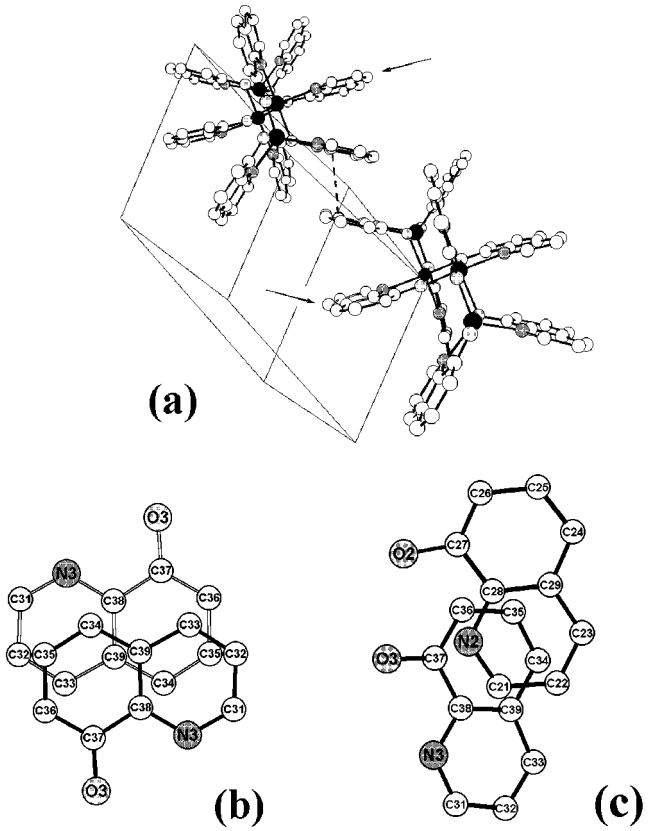

Figure 3. (a) Crystal $\pi-\pi$ stacking of $(Znq_2)_4$ molecules showing both intermolecular (indicated by dotted line) and intramolecular (indicated by arrows) interactions. Pyridyl/phenolato ring overlap is shown for (b) *inter*molecular interactions of bridging, terminal ligands and (c) *intra*-molecular interactions between bridging, terminal ligands and central ligands.

longest Zn−O bonds (2.176 Å) in the complex. This is ∼0.32 Å longer than the average Al−O bond in *mer*-Alq_3 and results in $\pi-\pi$ stacking of the pyridyl and phenolato moieties of adjacent 8-hydroxyquinoline ligands. This geometry differs significantly from *mer*-Alq_3, in which pyridyl/pyridyl ring overlap dominates.[7] However, we note that in the zinc tetramer the parallel ligands are offset by 1.39 Å (the measured shift between atoms C38 and C39) as shown in Figure 3b. These bridging, terminal ligands also exhibit intramolecular $\pi-\pi$ stacking with the central ligands of the tetrameric unit; however, in this case the pyridyl/phenolato ring overlap is weaker because of a large off-plane angle between the ligands of 23°. The closest interaction is 3.04 Å, which occurs between atom N2 of the central ligand and atom C37 of the terminal ligand (see Figure 3c). These inter- and intramolecular $\pi-\pi$ stacking interactions occur in the crystallographic [11$\bar{1}$] direction between molecules lined up along the crystallographic *b* axis and are 1-dimensional only. The closest interaction between the stacks is 8.6 Å along the *c*-crystallographic axis.

Table 2. Calculated Total Energies and Dipole Moments for the $(Znq_2)_n$ Series

$(Znq_2)_n$	SCF energy (au)	MP2 energy (au)	dipole moment[a] (D)
(Znq_2), monomer	2711.33648	2713.54660	6.840
$(Znq_2)_2$, dimer	5422.75456	5427.18320	0.994
$(Znq_2)_4$, tetramer	10845.57056		0.006

[a] Dipole moments given at the SCF level.

II. Tetramer Structural Stability. Structural parameters from our ab initio calculations on $(Znq_2)_4$ are summarized in Table 1. The basic structural unit of the tetramer crystal is a set of three adjoining, four-membered, Zn−O rings, which showed little distortion from planarity. Bond lengths and bond angles show good agreement with the experimental determination, but torsional parameters show greater variation. This results in a more open, less spherically compressed, structure, which is attributed to the absence of packing effects in the calculation.

In Table 2 we show the calculated total energies and dipole moments for the three molecules $(Znq_2)_n$ where $n = 1, 2, 4$, respectively. We note that $(Znq_2)_4$ is a lower energy configuration as compared to $2(Znq_2)_2$ by 38.6 kcal/mol. Furthermore, $(Znq_2)_2$ is energetically favored over $2Znq_2$ by 51.2 kcal/mol. The dimerization energy for Znq_2 at the MP2 level was 56.5 kcal/mol. While these energies do not include thermal and entropic effects, the overall magnitudes strongly suggest that the tetramer is thermodynamically favored over the monomer and dimer.

Experimental evidence for the stability and sole presence of the tetramer in crystalline Znq_2 was obtained from thermal analysis characterization. The DSC/TGA scans for crystalline $(Znq_2)_4$ are shown in Figure 4a. We observe a single endothermic transition at 361 °C with only a 2% weight loss prior to decomposition of the sample at ∼435 °C (see DDSC/DTGA curves in Figure 4b). Since there are differences in both the sizes and polarities of the Znq_2 monomer, dimer, and tetramer, based on calculated dipole moments, different melting points for these oligomers are expected. The DSC scans for crystalline $(Znq_2)_4$ measured at different heating rates are shown in Figure

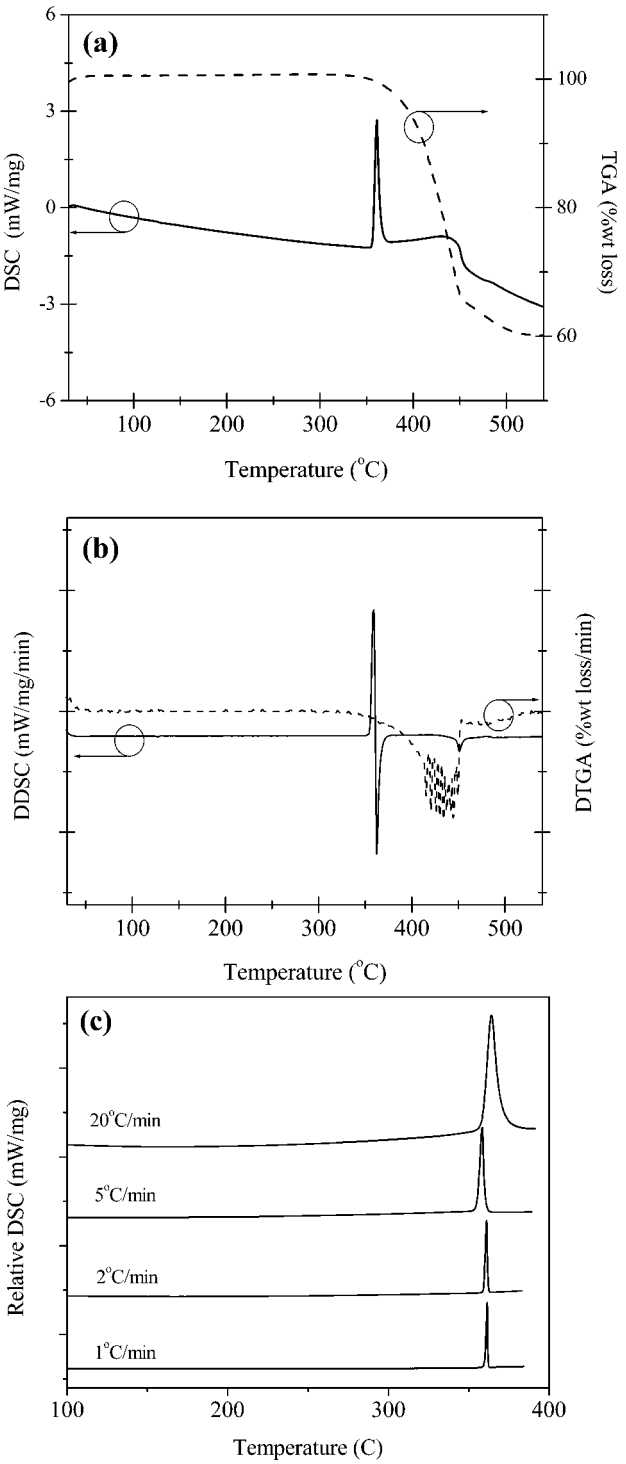

Figure 4. Thermal analysis characterization of $(Znq_2)_4$ showing (a) DSC/TGA curves (20 °C/min), (b) DDSC/DTGA curves (20 °C/min), and (c) DSC curves at different heating rates.

4c. A single endothermic transition ($\Delta H_{fusion} = \sim 50$ kcal/mol) was observed, which narrowed with decreasing heating rate. If smaller oligomeric species were present or formed by molecular rearrangement during fusion of $(Znq_2)_4$, additional enthalpic transitions would be expected to become resolved at slower heating rates. This behavior is in contrast to Alq_3, which shows several enthalpic transitions assigned to different polymorphic phases[7] and a simultaneous weight loss of ~15% attributed to sublimation.[14]

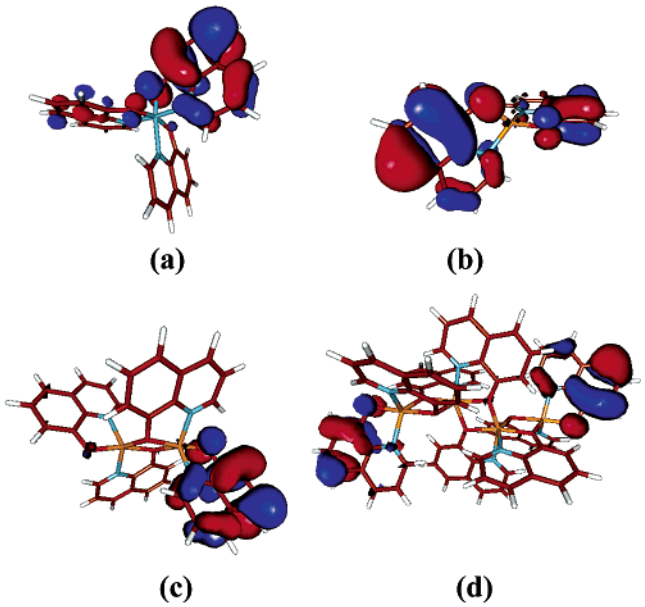

Figure 5. Orbital amplitude plots of the HOMO for (a) *mer*-Alq_3, (b) Znq_2 (monomer), (c) $(Znq_2)_2$ (dimer), and (d) $(Znq_2)_4$ (tetramer).

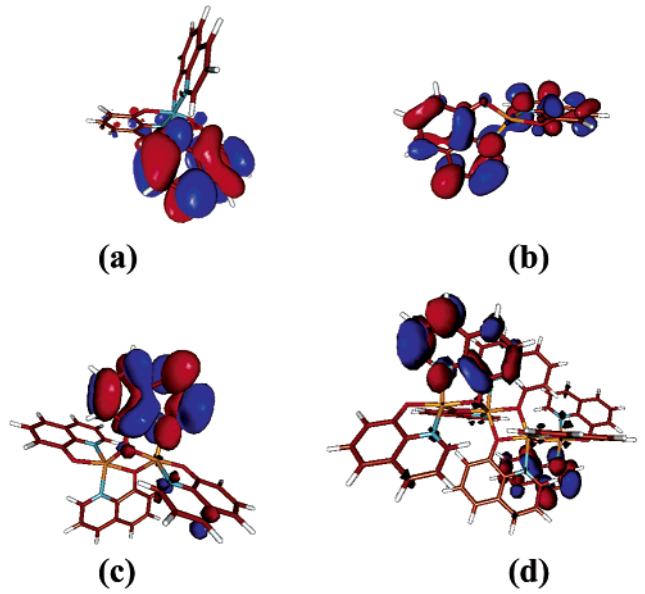

Figure 6. Orbital amplitude plots of the LUMO for (a) *mer*-Alq_3, (b) Znq_2 (monomer), (c) $(Znq_2)_2$ (dimer), and (d) $(Znq_2)_4$ (tetramer).

To access the stability of the tetrameric structure in vapor-deposited thin films, a sample of the crystalline $(Znq_2)_4$ was sublimed in a tube furnace (~10^{-6} Torr, up to 320 °C at 40 °C/min). Thermal analysis of the sublimed sample showed a single melting transition at a slightly lower temperature (359 °C) because of decreased crystallinity. Analysis of the crystalline and sublimed materials by ^{1}H NMR spectroscopy in $CDCl_3$ showed identical structures. Previously, we showed no detectable changes in the FT-IR spectra when comparing vapor-deposited films and the crystalline material dispersed in KBr.[15] These results support the stability of $(Znq_2)_4$, suggesting that films formed by thermal vapor deposition under high vacuum are likely composed solely of the tetrameric species.

III. Electronic Structure. In Figures 5 and 6 we compare the high-lying occupied and low-lying unoccupied molecular orbitals of *mer*-Alq_3 and the Zn chelate oligomers $(Znq_2)_n$. The

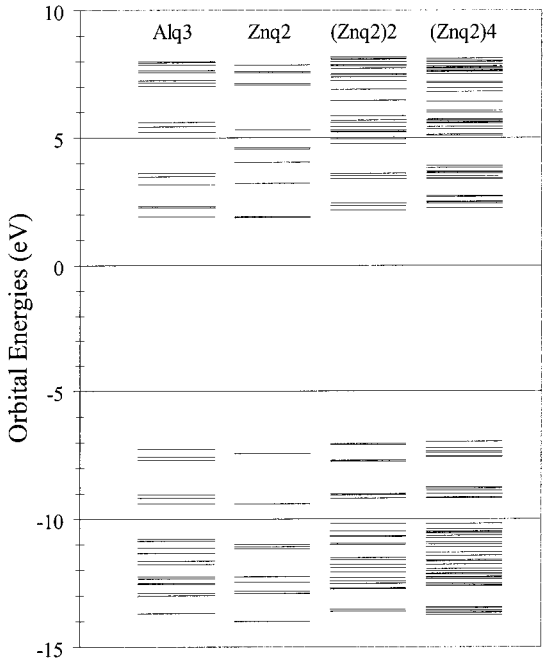

Figure 7. Calculated orbital energy level diagram for *mer*-Alq_3 and the $(Znq_2)_n$ oligomer series.

primary nodal patterns of the highest occupied molecular orbital (HOMO) and lowest unoccupied molecular orbital (LUMO) are dominated by orbitals originating from the 8-hydroxyquinoline ligands in all cases; however, the molecular orbitals of the $(Znq_2)_n$ oligomers are characterized by symmetry-related pairings.

Previous work for Alq_3 (both *mer* and *fac* isomers) has shown that the electron density of the HOMO is concentrated on the phenolato ring, and conversely is concentrated on the pyridyl ring for the LUMO.[5,10,12] A similar result is observed for the $(Znq_2)_n$ oligomers. However, relatively less electron density is observed on the pyridyl moiety in the cases of Znq_2 and $(Znq_2)_4$. This depletion of the pyridyl ring in the HOMO and LUMO is also observed for *fac*-Alq_3, and is likely a result of a decrease in localized character of the orbital amplitudes as symmetry is increased.[5] The inversion symmetry of the $(Znq_2)_4$ complex results in symmetry adapted pairs which localize the orbital amplitudes of the HOMO and LUMO into distinct spatial regions around different metal centers on opposite sides of the supramolecular structure. Specifically, the LUMO is localized on the two *bridging*, terminal ligands where the strong $\pi-\pi$ stacking interactions occur in the crystal, and the HOMO is localized on the two *nonbridging*, terminal ligands. However, the density shift from HOMO to LUMO still features ligand orbitals on the same metal center indicating Frenkel-like excitonic states similar to those observed in Alq_3.

An orbital energy level diagram comparing *mer*-Alq_3 and the $(Znq_2)_n$ series was constructed from the calculated orbital eigenvalues (see Figure 7). Although HF methods are well-known to provide poor prediction of the actual orbital energies resulting in a large overestimation of the HOMO/LUMO band gap, comparison of the differences between similar classes of materials can still be instructive.[34] Inspection of the energy level diagram shows that the lowest lying unoccupied and highest lying occupied orbitals group into "sets" corresponding to the

(34) Halls, M. D.; Schlegel, H. B. *Chem. Mater.* **2001**, *13*, 2632.

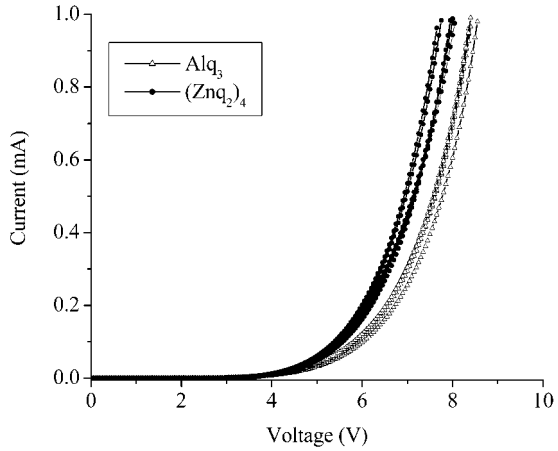

Figure 8. Current versus voltage plot for identically prepared Alq_3 and $(Znq_2)_4$-based OLEDs.

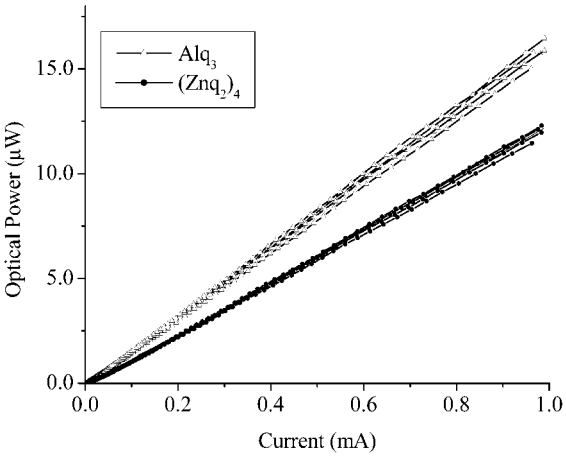

Figure 9. Light-output versus current plot for identically prepared Alq_3 and $(Znq_2)_4$-based OLEDs.

number of ligands in the complex [i.e.: triplet, Alq_3; doublet, Znq_2; quartet, $(Znq_2)_2$; and octet, $(Znq_2)_4$]. Preliminary near-edge X-ray absorption fine structure (NEXAFS) studies of $(Znq_2)_4$ thin films at the carbon and oxygen K-edges show a broadening of absorption bands compared to Alq_3 resulting from an increase in the number of atoms and unoccupied electronic states, which is consistent with a tetrameric structure for Znq_2.[25]

IV. Electroluminescent Properties. Identical OLEDs were prepared with Alq_3 and $(Znq_2)_4$ as the electron transporting/emissive layer. The current versus voltage characteristics of OLEDs composed of ITO/α-NPD/Mq_n/LiF−Al are shown in Figure 8. The device operating voltage is reported at a fixed current of 13mA/cm^2 (chosen to represent approximate video brightness) and was consistently lower for $(Znq_2)_4$-based OLEDs than for those made with Alq_3. The same trend was also observed for devices prepared with an Mg:Ag cathode, but with higher voltages for both $(Znq_2)_4$ and Alq_3. Figure 9 shows the dependence of the optical output power on drive current for the OLEDs. At a current of 100 μA, the EL output is $\sim$1.5$\times$ greater for Alq_3. These results are summarized in Table 3.

We speculate that the lower operating voltage for the $(Znq_2)_4$-based OLEDs is a consequence of the localization of the LUMO on the two bridging, terminal ligands involved in strong $\pi-\pi$ stacking of pyridyl/phenolato moieties providing a more efficient pathway for electron transport compared to Alq_3. The lower EL efficiency for $(Znq_2)_4$ is consistent with a significantly lower

Table 3. EL Data for the ITO/α-NPD/Metal Chelate/LiF/Al Device

metal chelate	voltage at 13 mA/cm^2	rel σ_{EL} ($Alq_3 = 1.00$)	rel power efficiency ($Alq_3 = 1.00$)
Alq_3	5.9	1.00	1.00
$(Znq_2)_4$	5.5	0.68	0.75

photoluminescent (PL) efficiency based on solution studies,[15,25] but may be even lower in the solid state. However, the C-4 methylated derivative of the zinc chelate ($4Meq_2Zn$) shows a large increase in PL efficiency compared to the unsubstituted analogue.[15,25] Similar behavior has been observed in the tris-(8-hydroxyquinoline) chelates of aluminum and gallium.[14] Thus we expect bis(4-methyl-8-hydroxyquinoline) zinc to provide the necessary balance between PL efficiency and charge transport for high-EL efficiency.

The consistently lower operating voltage exhibited by $(Znq_2)_4$-based devices suggests that it may be a superior electron transporting host for dye-doped OLEDs. However, since it is difficult to decouple the effects of bulk transport and injection we do not rule out the possibility of enhanced injection efficiency from the metal cathode into $(Znq_2)_4$ due to the behavior of interfacial dipoles as described by Baldo et al.[35] Previous studies of "electron only" devices of C-2 substituted ester derivatives of the zinc (8-hydroxyquinoline) chelate suggested that these materials had higher electron mobilities compared to Alq_3.[19] However, the molecular structures of those zinc chelates were not determined, but are more likely to have a monomeric structure. Oligomerization of zinc 8-hydroxyquinoline chelates might be controlled by selective substitution of the C2- or C7-positions of the ligand (next to nitrogen or phenolic oxygen) because of steric hindrance to metal chelation. Indeed, preliminary evaluation of 8-hydroxy-2-methylquinoline zinc(II) ($2Meq_2Zn$) showed large differences in photophysical and thermal properties compared to Znq_2 and other methylated derivatives, suggesting that $2Meq_2Zn$ is monomeric.[15,25] Structural and EL device characterization of the methylated derivatives of Znq_2 is in progress.

Conclusions

We presented a theoretical and experimental investigation of the molecular and electronic structure of the 8-hydroxyquinoline chelate of zinc(II) and related the results to OLED performance. Powder X-ray diffraction studies of the material purified by temperature gradient vacuum sublimation unequivocally showed that the structure of the chelate is tetrameric [$(Znq_2)_4$]. The sole existence of the tetrameric structure over smaller oligomeric species (monomer or dimer) was supported by both theoretical calculations of the total energies of the $(Znq_2)_n$ series and experimental thermal analysis and spectroscopic methods. It was shown that in contrast to the archetype EL material, Alq_3, the preferred crystal packing involves both close inter- and intramolecular $\pi-\pi$ interactions of ligands on adjacent molecules via pyridyl/phenolato ring overlap. Furthermore, calculation of the location and distribution of the HOMO and LUMO states by ab initio methods showed that the LUMO was localized on bridging, terminal ligands which are located on opposite sides of the tetrameric structure and are involved in $\pi-\pi$ stacking, leading to efficient electron transport through the molecules. These distinct, symmetry-induced differences between the molecular and electronic structures of $(Znq_2)_4$ and Alq_3 are correlated to the lower operating voltage observed for $(Znq_2)_4$-based OLEDs. Further improvements of EL performance might be achieved by control of the oligomerization of 8-hydroxyquinoline chelates of Zn(II) and/or by improving the PL efficiency by judicious substitution of the ligand as demonstrated previously for methylated Alq_3 and Gaq_3 chelates.[14]

Acknowledgment. The authors gratefully acknowledge financial support from NSF (CAREER-DMR-9874765), DOE Cooperative Agreement (DE-FC08-01NV14049), and PNNL Laboratory Directed Research and Development Project. K.F.F. acknowledges partial support by DARPA (Electroactive Coatings and Shutters for Protection of Sensors program, No. DAAD-19-99-1-0003). J.B. gratefully acknowledges summer support by the NSF-REU program. Pacific Northwest National Laboratory (PNNL) is operated by Battelle Memorial Institute for the U.S. Department of Energy (DOE) under Contract DE-AC06-76RLO 1830.

Supporting Information Available: Calculated structural parameters for the $(Znq_2)_n$ series ($n = 1, 2, 4$); FT-IR spectra of $(Znq_2)_4$ comparing samples prepared as KBr pellets and as vapor-deposited films on NaCl plates (PDF). This material is available free of charge via the Internet at http://pubs.acs.org.

JA0201909

(35) Baldo, M. A.; Forrest, S. R. *Phys. Rev. B* **2001**, *64*, 085201.